

Context-LGM: Leveraging Object-Context Relation for Context-Aware Object Recognition

Mingzhou Liu, Xinwei Sun[✉], Fandong Zhang, Yizhou Yu, and Yizhou Wang

Abstract—Context, as referred to situational factors related to the object of interest, can help infer the object’s states or properties in visual recognition. As such contextual features are too diverse (across instances) to be annotated, existing attempts simply exploit image labels as supervision to learn them, resulting in various contextual tricks, such as features pyramid, context attention, *etc.* However, without carefully modeling the context’s properties, especially its relation to the object, their estimated context can suffer from large inaccuracy. To amend this problem, we propose a novel Contextual Latent Generative Model (Context-LGM), which considers the object-context relation and models it in a hierarchical manner. Specifically, we firstly introduce a latent generative model with a pair of correlated latent variables to respectively model the object and context, and embed their correlation via the generative process. Then, to infer contextual features, we reformulate the objective function of Variational Auto-Encoder (VAE), where contextual features are learned as a posterior distribution conditioned on the object. Finally, to implement this contextual posterior, we introduce a Transformer that takes the object’s information as a reference and locates correlated contextual factors. The effectiveness of our method is verified by state-of-the-art performance on two context-aware object recognition tasks, *i.e.* lung cancer prediction and emotion recognition.¹

Index Terms—Object-context relation, Object recognition, Latent generative model, Variational Auto-Encoder, Transformer

I. INTRODUCTION

IN visual recognition, the object can vary along with its relating situational factors such as visual scene, which are collectively referred to as *context*. Therefore, context can provide helpful information to infer the object’s states or properties. Consider the benignity/malignancy classification of lung nodule, the malignant nodules can cause structure deformation (*e.g.* pleural indentation (Fig. 1-a) [1], vascular convergence (Fig. 1-b) [2]) through invasion and releasing chemical factors to their neighbors. As contextual signs, such deformation provides important cues for cancer diagnosis. Another common example is the recognition of facial emotion, where context can arise from the emotion sender (*e.g.*,

gesture (Fig. 1-c) [3], other people (Fig. 1-d) [4], and visual scene/objects (Fig. 5-v,w,s,y) [5].

Despite its importance, capturing context can be very challenging. This is because contextual factors can dramatically change across instances, in terms of pattern and location. Again, consider two types of structure deformation context in the malignant nodule, the pleural indentation and the vascular convergence, as examples. The pleural indentation context appears as a tangent line and locates at the margin of the nodule, while the vascular convergence context appears as several diffuse vessels pointing toward the nodule and locates in the nodule’s surrounding area. They differ significantly from each other in terms of pattern and location. Besides, the number of contextual factors can also vary a lot, *e.g.* some nodules present a single structure deformation, while others can cause multiple ones (Fig. 5-a,b) simultaneously.

As a result, it is intractable to annotate the “context” for supervised learning. Without annotations, existing methods exploit the image label as the only source of supervision to learn the context, resulting in a large literature of different contextual tricks, including but not limited to features pyramid [6], [7], atrous convolution [8], and the attention modules [9]–[18]. Although some of these methods showed performance improvements, they lacked careful modeling of context’s properties, especially its relation to the object. This inherent weakness limits their potentials to locate accurate context and achieve better performance.

Recently, psychology researches [19], [20] show that such an object-context relation is exploited by humans as common sense for recognition, as it can confuse human perceivers when the object and context are exposed incongruently. Inspired by this, we propose a novel **Contextual Latent Generative Model (Context-LGM)**, which models the object-context relation in a hierarchical perspective. Specifically, we firstly introduce a latent generative model coupled with a pair of correlated latent components to model the object and context, and embed their correlation via the generative processes. Then, guided by such modeling, we reformulate the Evidence Lower **BO**und (ELBO) of Variational Auto-Encoders (VAE) as objective function to infer object’s and contextual features. Particularly, the posterior of contextual features is conditioned on the object, in order to take the object’s information as a reference. Finally, to implement it, we introduce a contextual posterior Transformer [21]. With careful modifications, we show our Transformer can screen out environmental factors correlated to the object, and well handle the diversity of context.

To verify the utility of our Context-LGM, we evaluate it on two context-aware object recognition tasks, namely lung

[✉]indicates corresponding authors.

Mingzhou Liu is with Computer Science Department, Peking University, 100871, Beijing, China (e-mail: liumingzhou@stu.pku.edu.cn).

Xinwei Sun is with Microsoft Research Asian, Beijing, 100080, China (e-mail: xinsun@microsoft.com).

Fandong Zhang is with DeepWise AI Lab, Beijing, 100080, China (zhangfdxk@163.com).

Yizhou Yu is also with DeepWise AI Lab, Beijing, 100080, China (yizhouy@acm.org).

Yizhou Wang is with Computer Science Department, Peking University, 100871, Beijing, China (e-mail: yizhou.wang@pku.edu.cn).

¹Codes will be made available after acceptance.

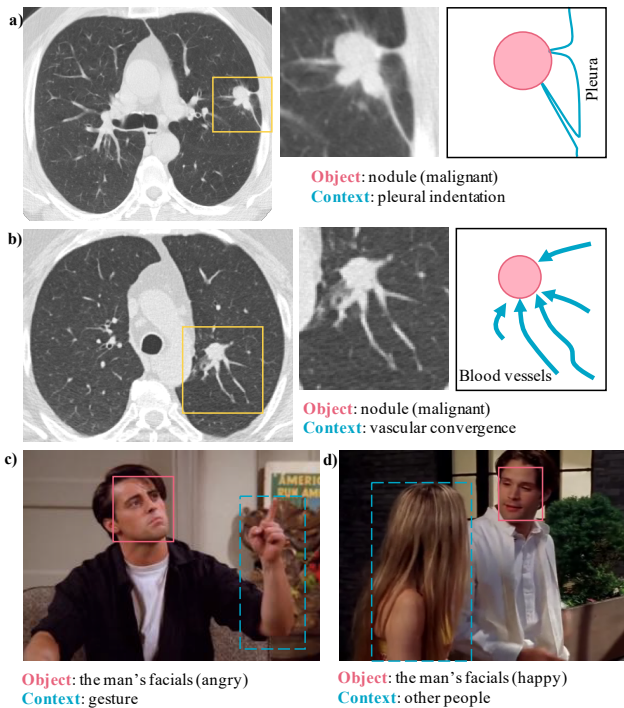


Fig. 1. Examples of objects and their correlated contextual features. (a) a malignant lung nodule that causes pleural indentation; (b) a malignant lung nodule with vascular convergence; (c) a man with angry facials and gestures; (d) a man with happy facials for meeting other people. Background knowledge for context in lung cancer is available in Appendix A.

cancer prediction and emotion recognition. It yields that our method achieves state-of-the-art performance with significant margins. Besides, the visualization results qualitatively show that our method can locate interpretable context.

In summary, our contributions are:

- **Ideologically**, we are the *first* to incorporate object-context relation into context-aware object recognition.
- **Methodologically**, we propose a novel latent generative model that embeds object-context relation in the generating process of two coupled latent variables.
- **Algorithmically**, we reformulate the ELBO of VAE as objective function and implement a contextual posterior Transformer to infer contextual features.
- **Experimentally**, we achieve state-of-the-art performance in two context-aware object recognition tasks.

The preliminary version of this work has been accepted by MICCAI-2021 [22]. This paper extends the initial version in significant ways. **Firstly**, we propose a latent generative framework to carefully model context, especially its relation to the object. **Secondly**, we reformulate the ELBO of VAE and infer contextual features as a posterior distribution conditioned on the object. **Thirdly**, we modify the Transformer to implement this contextual posterior. **Finally**, we extend experiments to emotion recognition and provide more comprehensive results.

The rest of the paper is organized as follows: Section II gives a brief review of related works; Section III gives the detailed generative modeling, ELBO reformulating, and Transformer architecture of Context-LGM; Section IV provides

quantitative and qualitative experimental results; Section V concludes the paper and discusses future works.

II. RELATED WORKS

A. Context-Aware Object Recognition

Many context-aware methods have been proposed in visual recognition, such as [6]–[18]. The main focus lies in identifying context from complicated surrounding scenarios. To achieve this goal, existing methods follow the paradigm of using only image labels to capture context. Their typical designing tricks include features pyramid, atrous convolution, and attention modules.

The features pyramid [6], [7] and atrous convolution [8] were designed to enlarge the receptive fields and avoid missing context with extreme sizes or locations. Recently, the attention mechanism has become a new dominance for context modeling [9]–[18]. In these methods, various types of context attention implementations, including spatial-wise attention [9], [12]–[14], channel-wise attention [11], [16]–[18], spatial-channel wise attention [10], and graph-based attention [15], were exploited to select label-correlated context and suppress other irrelevant backgrounds.

However, without further careful modeling of context’s properties, especially its relation to the object, their learned context can suffer from large inaccuracy. Using even more designing tricks can not overcome these inherent obstacles they face. **In contrast**, our Context-LGM uses a pair of correlated latent variables to model the object and context, as well as the correlation between them. During inferring contextual features, we additionally incorporate the object’s information as a reference. Such careful modeling of context and its relation to the object enable our methods capture better contextual representations, thus benefit the recognition.

B. Latent Generative Model

The latent generative model starts with a Bayesian Network, which introduces latent variables that are characterized via their generating processes. The simplest example is $z \rightarrow x$, in which z denotes the latent variables that generate x . The goal is learning $p(x)$, which is however intractable for maximum likelihood based method if x is high-dimensional (*e.g.*, x denotes image). The Variational Auto-Encoder (VAE) proposed the Evidence Lower Bound (ELBO) as a surrogate and tractable objective, by introducing the variational distribution $q(z|x)$ that is easy for sampling.

Not only as a generator, the VAE can also be used to infer the latent representations from x . Specifically, it adopts the (variational) Encoder and Decoder, which respectively infer z from x and generate x from z . There is a large literature in VAE to learn such meaningful representations [23]–[26]. Specifically, the [23], [24], [27] proposed to learn disentangled representations. Particularly, the [26], [28] considered the supervised learning tasks and split the latent variables into two parts that were modeled differently. Benefited from its tractability and the ability to infer latent variables, we adopt the VAE framework to model the correlation between object and context via their latent generating processes. We then

reformulate the ELBO based on the corresponding Bayesian Network. To the best of our knowledge, we are the *first* to model contextual features and exploit its relation to the object of interest during inference. Our experimental results will show that such modeling can significantly improve the performance and learn interpretable context.

C. Transformer

Transformer [21] was initially proposed in natural language processing (NLP). Equipped with its unique multi-head attention in the self/cross-attention block, it can well model both the short-term and long-term dependencies among word tokens and thus achieves remarkable performance on various NLP tasks. Recently, Transformer and its attention mechanism have been introduced into visual relationships modeling, such as pixel-level dependencies in image classification [29], [30] and segmentation [31]–[33], relationships among proposals in detection [34], correlation among keypoints in pose estimation [35], [36], and temporal correspondence in tracking and action recognition [37], [38].

In our scenario, we implement a Transformer to model object-context correlation and infer contextual representations. To fit our task, we make careful modifications to the original designs. Specifically, we inherit the multi-head attention in the cross-attention block but implement it in a spatial-wise masking manner. This modification allows us to use the learned object-context correlation as a spatial mask and screen out contextual factors that are correlated with the object. Besides, we remove the Encoder-Decoder structure that is specifically designed for sequence-to-sequence translation. We also reduce the number of stacked attention layers and remove all FFNs to improve computational efficiency.

III. METHODOLOGY

Problem Setup & Notation. Our goal is to predict object’s state/label y (e.g., benignity/malignancy or emotion) given an observed image x . The training data contains $\{x_i, y_i\}_i$ *i.i.d* $p(x, y)$. In the graph of generative model, we use “o” as a metasymbol to represent any kind of ends: ’>’, ’<’, and the empty mark,. That is, the a o-o b can represent $a \rightarrow b$, $a \leftarrow b$, or the missing link between a and b . The $a \rightarrow b$ means b is generated after a . We use x, x, X to respectively denote the random variable, its instance and the matrix.

In this section, we introduce **Contextual Latent Generative Model (Context-LGM)** from a hierarchical perspectives of generative modeling (in section III-A), objective reformulation (in section III-B) and finally, the Transformer (in section III-C) for implementation. Specifically, in section III-A, we firstly introduce the Bayesian Network and its encoded generative processes related to the object and context. Then, in section III-B, we derive a reformulated ELBO as our objective function in the VAE framework to infer the object’s and contextual features for prediction. Particularly, the posterior of contextual features is conditioned on the object’s features, in order to take the object’s information as a reference. Finally, in section III-C, we implement a contextual posterior Transformer with a carefully modified cross-attention block to optimize the above posterior model.

A. Contextual Generative Modeling

We introduce three latent variables z_o, z_c, z_b to respectively model the object’s, contextual and other background features. Together with the observed image x and object’s state/label y , their generating processes are illustrated by the Bayesian Network in Fig. 2(a). As shown, the z_o, z_c, z_b all participate in generating the image x , with each one responsible for corresponding source of variation in the whole image. Only z_o, z_c are related to the label y . As an intuitive example, consider the man with angry facials and gesture in Fig. 1(c). The y denotes his angry emotion, the z_o models his facial expressions, the z_c models his gesture context, and the z_b models the other emotion-irrelevant backgrounds such as the door, sofa, etc.

More importantly, the object’s features z_o is correlated to the contextual features z_c via their generating processes, as shown by the unblocked path between z_o and z_c in Fig. 2(a). This path is composed of $y \rightarrow z_o$ (i.e., the object’s state y generates its features z_o), z_o o-o z_c and z_c o-o y . It includes but not limited to the following possible types:

- $y \rightarrow z_o, y \rightarrow z_c$, missing link between z_o and z_c that corresponds to “Type I” in Fig. 2(a). In this case, the object’s state y co-generates object’s features z_o and contextual features z_c . For example, one can express his/her angry via simultaneous changes of facial expressions and body gestures.
- $y \rightarrow z_o, y \rightarrow z_c$ and $z_o \rightarrow z_c$ that corresponds to “Type II” in Fig. 2(a). In this case, the generation of context z_c is not only influenced by object’s state y , but also directly by the object z_o . For example, the structure deformation context is caused not only by the malignant nature of nodule, but also by its invasion pattern.
- $z_c \rightarrow y, z_c \rightarrow z_o$, and $y \rightarrow z_o$ that corresponds to “Type III” in Fig. 2(a). In this case, environmental context z_c influence the generation of object’s state y and features z_o . For example, scene objects and other people can influence the experience and expression of emotion [39]

Regardless of the types of path between z_o and z_c , the label y and latent variables z_o, z_c , and z_b obey the following properties: **i)** only z_o, z_c are related to y ; **ii)** z_o is related to z_c . Mathematically speaking:

$$\begin{aligned} y \perp z_o | z_c; \quad y \perp z_c | z_o; \quad z_o \perp z_c; \\ z_b \perp y | z_o, z_c; \quad z_b \perp z_o; \quad z_b \perp z_c; \end{aligned} \quad (1)$$

These properties composite the cornerstone for the learning of object’s and contextual representations, which we will introduce in the subsequent section.

B. Learning Method

Guided by the Bayesian Network in Fig. 2(a) and the properties derived in Eq. (1), we introduce our method to infer z_o and z_c for prediction, by reformulating the ELBO of VAE. Specifically, the ELBO with $q_\phi(z|x)$ ($z := [z_o, z_c, z_b]$) for simplicity) as variational distribution is:

$$\log p(y, x) \geq \log p_\psi(y|x) + \mathbb{E}_{q_\phi(z|x)} \log \frac{p_\psi(x|z)p(z)}{q_\phi(z|x)}, \quad (2)$$

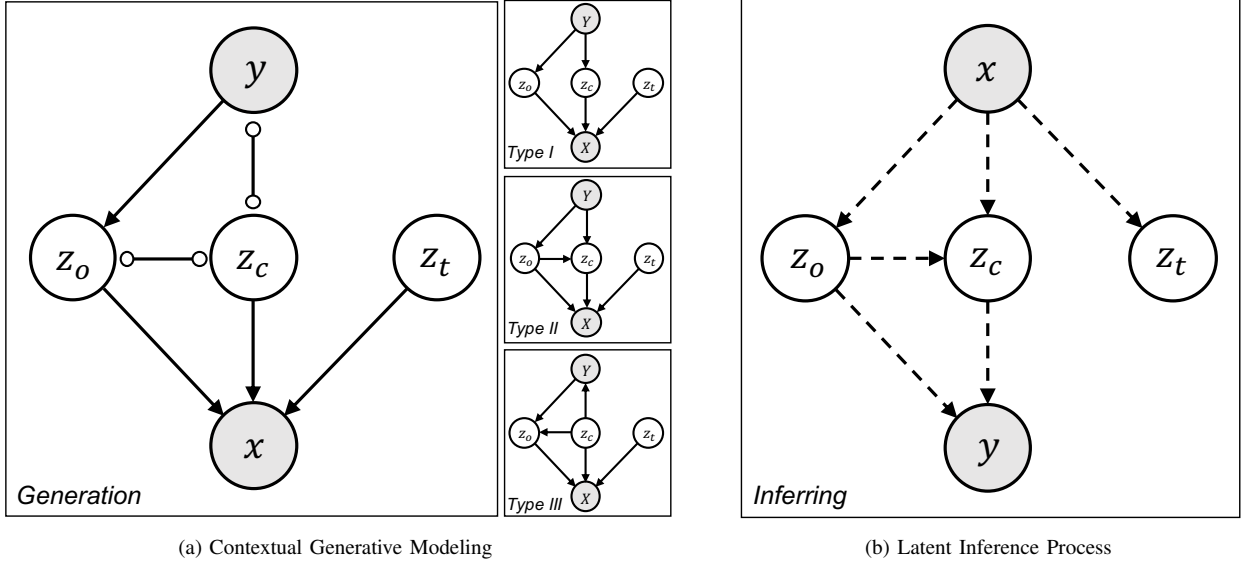


Fig. 2. (a) Contextual generative modeling. The o-o mark denotes \rightarrow , \leftarrow , or the missing link. We argue that an observed image is generated from three latent variables, *i.e.*, z_o , z_c , and z_b . These three variables respectively model the target object, context, and background features. More importantly, the object z_o and context z_c are correlated via their generative process. Specifically, they can be co-generated from y (Type-I); Also, the object z_o can also have direct influence on generating context z_c (Type-II); Besides, the environmental context z_c can generate the object's state y and its features z_o (Type-III). (b) Latent inference process. Given the observed image x , we firstly infer object's latent z_o since the object is with annotations and easier to learn. Then, we infer contextual latent z_c from x using object's information z_o as a reference. Finally, z_o and z_c are jointly used to infer object's label y . The white variable means unobserved variable, shaded variable means observed one.

where $q_\phi(z|x)$ is the variational distribution.

We further approximate the $p_\psi(y|x)$ as:

$$p_\psi(y|x) \approx \int p_\psi(y|z)q_\phi(z|x)dz. \quad (3)$$

Then, the optimization for Eq. (2) involves the posterior model $q_\phi(z|x)$, the recognition model $p_\psi(y|z)$, the generation model $p_\psi(x|z)$, and the prior $p(z)$. The overall inference process and the network structure are respectively shown in Fig. 2 (b) and Fig. 3.

Posterior Model. For the posterior $q_\phi(z|x)$, we adopt the mean field approximation for the following factorization:

$$q_\phi(z|x) = q_\phi(z_o, z_c|x)q_\phi(z_b|x). \quad (4)$$

To leverage the object-context correlation, we incorporate the object's information as a reference during inferring z_c :

$$q_\phi(z_o, z_c|x) = q_\phi^c(z_c|z_o, x)q_\phi^o(z_o|x), \quad (5)$$

with $q_\phi^o(z_o|x) \sim \mathcal{N}(\mu(x), \Sigma(x))$, and $q_\phi^c(z_c|z_o, x) \sim \mathcal{N}(\mu(z_o, x), \Sigma(z_o, x))$. To implement it, the object's posterior network $q_\phi^o(z_o|x)$ is parameterized by a backbone network followed by a Region-Of-Interest (RoI) pooling layer. The contextual posterior $q_\phi^c(z_c|z_o, x)$ is parameterized by the same backbone network, followed by a RoI masking layer and a contextual posterior Transformer. The detailed architecture of our Transformer will be introduced in the subsequent section.

Recognition Model. The recognition item has $p_\psi(y|z) = p_\psi(y|z_o, z_c)$, due to the independence between y and z_b in Eq. (1). The $p_\psi(y|z_o, z_c)$ is parameterized by a early concatenation of (z_o, z_c) followed by a three-layers fully connected classifier.

Generation Model. The generation model for image $p_\psi(x|z)$ is parameterized by a convolution layer followed by four-layer de-convolution layers.

Objective Function. With Eq. (3), (4), (5), the final loss is:

$$\mathcal{L}_{\phi, \psi} = \frac{1}{n} \sum_{i=1}^n \left(-\lambda_1 \log p_\psi(y_i|z_o, z_c)q_\phi^c(z_c|z_o, x_i)q_\phi^o(z_o|x_i) + \lambda_2 D_{\text{KL}}(q_\phi(z|x_i), p(z)) - \lambda_3 \mathbb{E}_{q_\phi(z|x_i)} \log p_\psi(x_i|z) \right). \quad (6)$$

where n denotes samples number in our dataset. λ_1 , λ_2 , and λ_3 respectively denote ratios for recognition loss, KL divergence loss, and reconstruction loss.

Training & Test. We optimize over $q_\phi(z|x)$, $p_\psi(x|z)$ and $p_\psi(y|z_o, z_c)$ by minimizing Eq. (6) in the training stage. During test stage, we firstly infer z_o via $q_\phi^o(z_o|x)$. Then, we infer z_c via $q_\phi^c(z_c|z_o, x)$. Finally, we feed the inferred z_o and z_c into the recognition model $p_\psi(y|z_o, z_c)$ to predict y .

C. Contextual Posterior Transformer

Overview. Fig. 3 shows an overview of our Transformer. As we can see, we inherit the multi-head attention mechanism as our core implementation of object-context correlation, due to its ability on modeling various aspects of relationships. To adapt the Transformer well into our visual recognition task, we make the following modifications to the original designs:

- For the implementation of attention function in the cross-attention block, we replace the dot-product transformation attention (that is originally designed for source-target language translation) with a Hadamard product spatial-wise attention, to screen out those features that are highly correlated to the object.

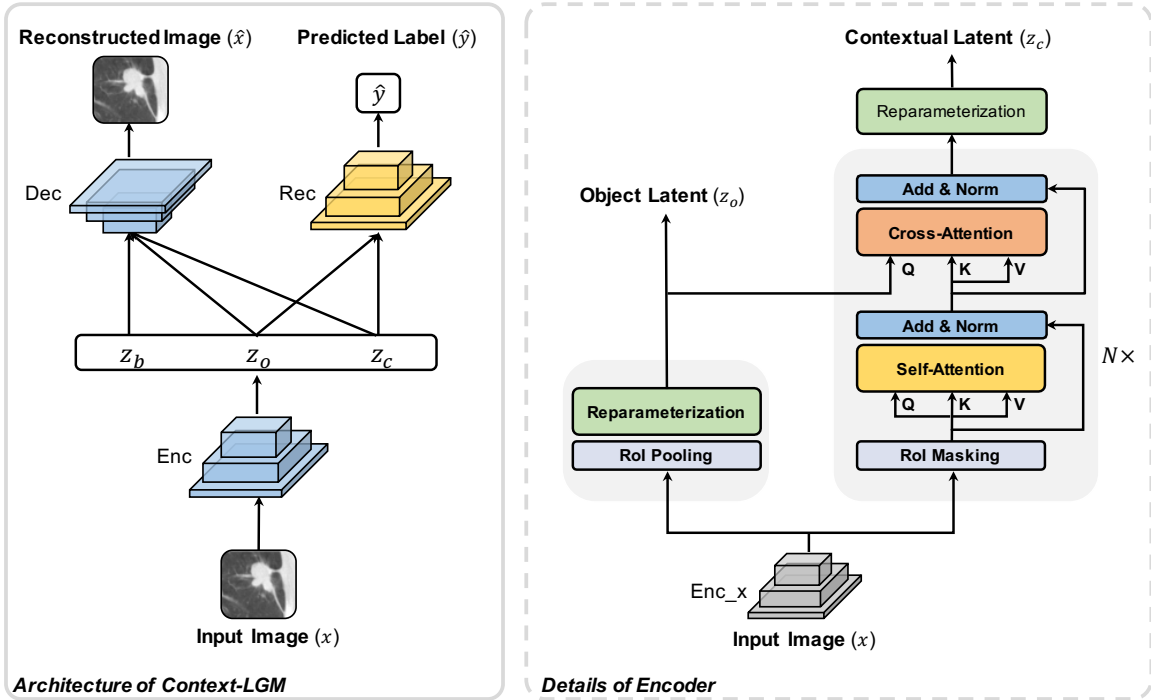


Fig. 3. Left: network structure of the proposed Context-LGM. Given the input image x , the Encoder (Enc) firstly extracts latent representations for the object (z_o) and its context (z_c). Then, the Decoder (Dec) takes z_o, z_c , and z_b as input and outputs a reconstructed image \hat{x} ; The Recognition Net (Rec) takes z_o and z_c as input and outputs the predicted label \hat{y} . Right: the structure of posterior model $q_{\phi}^c(z_o, z_c|x)$. It feeds x into a backbone feature extractor (Enc_x) and obtains deep feature maps F . To obtain z_o , F is fed into a Region-Of-Interest (RoI) pooling layer followed by a reparameterization. To obtain z_c , the masked-RoI feature maps F_{mask} is fed into a contextual posterior Transformer. The Transformer consists of N compositions of attention layers. Each attention layer contains a self-attention block and a cross-attention block. The self-attention block aims to mutually enhance features representation, while the cross-attention block takes the object's information z_o to select correlated context z_c .

- We remove the Encoder-Decoder structure that is specifically designed for the sequence-to-sequence translation but is not required in our task.
- we reduce the number of stacked attention layers and remove all FFNs. These can improve computational efficiency without loss of accuracy.

Multi-Head Attention Function. Attention function is the cornerstone in Transformer. Given the input query $\mathbf{Q} \in \mathbb{R}^{N_q \times C}$, key $\mathbf{K} \in \mathbb{R}^{N_k \times C}$, and value $\mathbf{V} \in \mathbb{R}^{N_v \times C}$ (N_q, N_k, N_v respectively denotes token length for query, key, and value, C denotes channel dimension), the attention function is defined as a dot-product between affinity matrix $\mathbf{A}_{qk} = \mathbf{Q}\mathbf{K}^T$ and \mathbf{V} :

$$\text{Attention}(\mathbf{Q}, \mathbf{K}, \mathbf{V}) = \text{Softmax}_{col}\left(\frac{\mathbf{A}_{qk}}{\tau}\right)\mathbf{V} \quad (7)$$

where τ is a temperature parameter controlling the softmax distribution, col denotes softmax is performed column wise.

In our scenario, the contextual features can present multiple patterns/locations/quantities. So, we also extend the attention function in Eq.(7) into multi-head attention [21] to enhance its ability on modeling various aspects of contextual correlations. Specifically, the multi-head function is defined as:

$$\begin{aligned} \text{MultiHead}(\mathbf{Q}, \mathbf{K}, \mathbf{V}) &= \text{Concat}(\mathbf{H}_1, \mathbf{H}_2, \dots, \mathbf{H}_{n_h}) \\ \mathbf{H}_i &= \text{Attention}(\mathbf{Q}\mathbf{W}_i^Q, \mathbf{K}\mathbf{W}_i^K, \mathbf{V}\mathbf{W}_i^V) \end{aligned} \quad (8)$$

where n_h denotes head numbers; $\mathbf{W}_i^Q \in \mathbb{R}^{C_q \times C_{q_i}^Q}$, $\mathbf{W}_i^K \in \mathbb{R}^{C_k \times C_{k_i}^K}$, and $\mathbf{W}_i^V \in \mathbb{R}^{C_v \times C_{v_i}^V}$ are learned parameter metrics

for query, key, and value; $C_{q_i}^Q = \frac{C_q}{n_h}, C_{k_i}^K = \frac{C_k}{n_h}, C_{v_i}^V = \frac{C_v}{n_h}$. We share weight between \mathbf{W}_i^Q and \mathbf{W}_i^K , as it has been suggested [37] to embed the (query, key) into the same space and help accurate correlation computing.

Self-Attention Block. The self-attention block aims to mutually enhance feature maps representations. It takes the masked RoI feature maps $\mathbf{F}_{mask} \in \mathbb{R}^{H \times W \times C}$ (H, W denote spatial dimensions, and C denotes channel dimension) as input. We reshape \mathbf{F}_{mask} into $\mathbb{R}^{C \times N}$ ($N = H \times W$) by flattening the spatial dimensions and feed it in into the multi-head attention function. The output of the attention is added to the input feature maps as a residual item:

$$\mathbf{F}_{self} = \text{Norm.}(\text{MultiHead}(\mathbf{F}_{mask}, \mathbf{F}_{mask}, \mathbf{F}_{mask}) + \mathbf{F}_{mask})$$

where Norm. denotes a normalization layer and \mathbf{F}_{self} denotes output of self-attention block.

Cross-Attention Block. As our key implementation of the object-context correlation, the cross-attention block leverages the object's information as guidance in learning the contextual representations.

Specifically, it takes both object's latent z_o and the output of self-attention block \mathbf{F}_{self} as input. In its multi-head attention function, the object's latent z_o is used as query and \mathbf{F}_{self} is used as key and value, such that feature tokens in \mathbf{F}_{self} with high correlation to z_o can be enhanced and those with low correlations can be suppressed:

$$\mathbf{F}_{cross} = \text{Norm.}(\text{MultiHead}(z_o, \mathbf{F}_{self}, \mathbf{F}_{self}) + \mathbf{F}_{self})$$

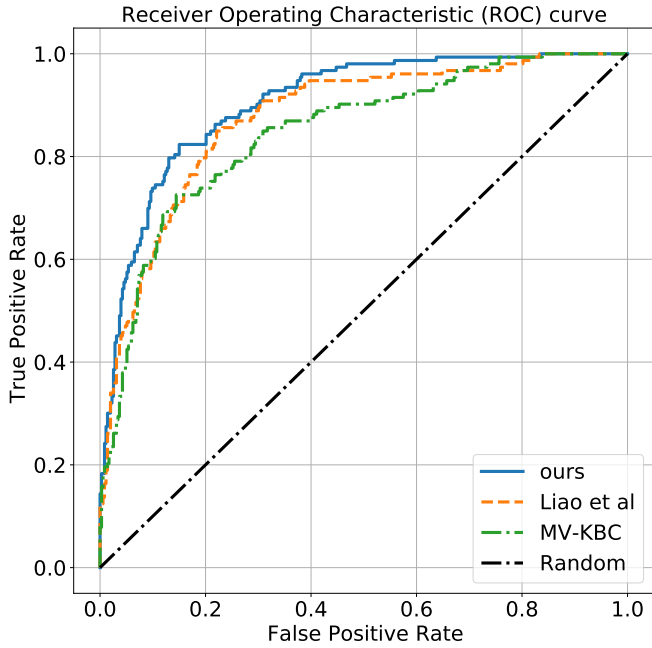


Fig. 4. ROC curves of different methods in lung cancer prediction task. Note that detailed prediction probability for each data point is required to draw ROC curves. So only baseline methods with official training codes or model weights are included for fairness.

The contextual latent z_c is then estimated by a reparameterization on \mathbf{F}_{cross} .

Note that originally, the attention in Eq. (7) is implemented by a dot-product between affinity \mathbf{A} and value \mathbf{V} , such that the source sentence (\mathbf{V}) can be transformed into target language (\mathbf{Q}) domain according to words correspondence (\mathbf{A}). However, as mentioned earlier, our cross-attention block aims to emphasize environmental factors with high correlation to the object and suppress those with low correlation. Hence, we implement our cross-attention in a spatial-wise attention manner:

$$\text{Attention}(\mathbf{Q}, \mathbf{K}, \mathbf{V}) = \text{Softmax}_{col}\left(\frac{\mathbf{M}_{qk}}{\tau}\right) \odot \mathbf{V} \quad (9)$$

with $\mathbf{M}_{qk} := \sum_{row} A_{qk}$, as the spatial-wise object-context correlation matrix. “ \sum_{row} ” means the summation is performed row-wise and \odot denotes a Hardmard product.

During the Hardmard product, the left spatial correlation item is a $N_k \times 1$ matrix, and the right value item \mathbf{V} is a $N_k \times C$ matrix. The spatial correlation is shared among different channel dimensions.

IV. EXPERIMENTS

In this section, we report quantitative and qualitative results of the proposed Context-LGM on two context-aware object recognition tasks, *i.e.* lung cancer prediction, and emotion recognition. Correspondingly, in lung cancer prediction, the contextual features include structure deformations/attachments by nodules; In emotion recognition, they include gestures, scene/objects, or other people.

A. Datasets and Evaluation Metrics

Lung Cancer Prediction. The Data Science Bowl (DSB) 2017 dataset [58] in Kaggle’s competition is used. This dataset provides a pathologically confirmed lung cancer label for each patient. There are 1397, 198, and 506 patients in the training, validation, and test set, respectively. We report official evaluation metrics including the Receiver Operating Characteristic (ROC) curve, the Area Under ROC curve (AUC), and the Log Loss (also known as the cross-entropy loss). The various types of contextual features (*i.e.*, structure distortions, attachments) and its relation to the nodule is illustrated in Fig. 8(b-g).

Emotion Recognition. The Context-Aware Emotion Recognition (CAER-S) dataset [43] is used. This dataset contains 48,971 images for training and 20,954 images for validation. Each image is assigned to one of the seven emotion categories (neutral, happy, sad, surprise, fear, disgust, and angry) based on people’s facial expressions and context. We report its official evaluation metric, *i.e.* Top-1 Accuracy (Acc). The context specifically denotes gestures, scene/objects, and other people, as marked by the dash blue boxes in Fig. 5 (i-y).

B. Implementation Details

For both tasks, we implement SGD for optimization, with momentum set to 0.9 and weight decay to 0.0001.

Lung Cancer Prediction. Given CT image x and cancer label $y \in \{0, 1\}$, we implement an off-the-shell nodule detector [42] to detect all nodules $\{N_1, N_2, \dots, N_n\}$ in the patient. For each nodule N_i , an $96 \times 96 \times 96\text{mm}^3$ patch containing both nodule and surroundings is cropped and feed into Context-LGM to predict a malignancy score \hat{y}_i . Based on all nodules’ malignancy probabilities $\{\hat{y}_1, \hat{y}_2, \dots, \hat{y}_n\}$, the predicted cancer probability is defined by $\hat{y} = 1 - \prod_{i=0}^n \hat{y}_i$.

Our backbone is a 3D U-Net. Data pre-processing includes pixel space re-sampling ($1 \times 1 \times 1\text{mm}^3$), intensity normalization (window center HU= -600, window width HU= 1600), and lung segmentation. Data augmentations include random flipping, resizing, rotation and shifting. Alternative training on classification and detection is used to alleviate over-fitting.

In the contextual posterior Transformer, short cuts between each attention layer are used to alleviate gradients vanishing as suggested by [59]. Channel dimension C is 128. The heads number is set to 4, the layers number is set to 2, τ is set to 30. The training takes 60 epochs, with the learning rate set to 0.01 and decreases by a factor of 0.1 at epoch 20, 35. We multiply the learning rates for modules other than the backbone by a factor of 1.25 in the first 20 epochs to promote faster convergence. Due to GPU memory constraints, the batch size is set to 12. The $\lambda_1, \lambda_2, \lambda_3$ in Eq. (6) for recognition loss, KL divergence loss, and reconstruction loss are all set to 1.0. It takes eight hours to train on two Nvidia Tesla V100 GPUs.

Emotion Recognition. We first crop the target face in each image and resize it into 96×96 . We then mask the target face (by zero paddings) and resize its surrounding areas into 140×160 . We tried various backbones: 5-layers CNN adopted in [43]–[45] and ResNet-18 adopted in [46]–[49]. Data augmentations include random cropping (128×128) and flipping.

Method	Publish	Context	AUC(%) \uparrow	LogLoss \downarrow
grt123		\checkmark	-	.3998
J. de Wit & D. Hammack		\checkmark	-	.4012
Aidence	Competition	-	-	.4013
qfpxfd		-	-	.4018
Pierre Fillard		-	-	.4041
MV-KBC [40]	TMI 18	\times	84.67	.4887
Ozdemir <i>et al.</i> [41]	TMI 19	\checkmark	86.90	-
Liao <i>et al.</i> [42]	TNNLS 19	\checkmark	87.00	.3989
ours		\checkmark	90.24 \pm 0.16	.3836 \pm .0065

TABLE I

COMPARISON RESULTS OVER OTHER METHODS IN LUNG CANCER PREDICTION TASK. ‘CONTEXT’ DENOTES WHETHER CONTEXT INFORMATION IS CONTAINED IN THE INPUT IMAGE. ‘-’ MEANS UNAVAILABLE. OUR RESULT IS REPORTED IN MEAN \pm STD. STANDARD VARIANCE FOR BASELINE METHODS ARE NOT REPORTED IN THEIR PAPERS.

Backbone	Method	Publish	Context	Acc(%) \uparrow
5-Layers CNN	CAER-Net [43]	ICCV 19	\checkmark	77.83*
	Jaiswal <i>et al.</i> [44]	UPCON 2020	\checkmark	81.00
	Zeng <i>et al.</i> [45]	CSRSWTC 2020	\checkmark	81.31
	ours		\checkmark	85.30 \pm 0.07
ResNet-18	SIB-Net [46]	IJCB 21	\checkmark	74.56
	Li <i>et al.</i> [47]	TAC 21	\checkmark	84.82
	EfficientFace [48]	AAAI 21	\times	85.87
	MA-Net [49]	TIP 21	\times	88.42
	ours		\checkmark	91.36 \pm 0.05

TABLE II

COMPARISON RESULTS IN EMOTION RECOGNITION TASK. EFFICIENTFACE [48] USED RESNET-50 AS BACKBONE. * DENOTES OUR RE-TRAINING RESULT, ORIGINAL RESULT IS 73.51%. ‘CONTEXT’ DENOTES WHETHER CONSIDERING CONTEXT INFORMATION. OUR RESULT IS REPORTED IN MEAN \pm STD. STANDARD VARIANCE FOR BASELINE METHODS ARE NOT REPORTED IN THEIR PAPERS.

vanilla		ours		DSB2017	CAER-S
object	context	VAE	Transformer	AUC(%) \uparrow	Acc(%) \uparrow
\checkmark				88.06 \pm 0.67	71.89 \pm 0.26
\checkmark	\checkmark			88.72 \pm 0.15	76.96 \pm 0.17
\checkmark	\checkmark	\checkmark		88.88 \pm 0.02	80.27 \pm 0.14
\checkmark	\checkmark	\checkmark	\checkmark	90.24 \pm 0.16	85.30 \pm 0.07

TABLE III

ABLATIVE STUDY OF OUR METHOD. VANILLA OBJECT/CONTEXT MEAN THEY ARE DIRECTLY LEARNED VIA CROSS ENTROPY.

Our contextual posterior Transformer takes fusion of multi-levels backbone feature maps as input. Channel dimension C is 256, heads number is set to 2, layer number is set to 1, and τ is set to 30. The training takes 85 epochs, with the learning rate set to 0.01 and decrease by a factor of 0.1 at epoch 55. The batch size is set to 128. The $\lambda_1, \lambda_2, \lambda_3$ in Eq. (6) for recognition loss, KL divergence loss, and reconstruction loss are set to 1.0, 0.1, 1.0, respectively. It takes five hours to train on one Nvidia Tesla V100 GPU.

C. Results Analysis

Lung Cancer Prediction. We compare our method with baselines from Kaggle’s competition leader board and other state-of-the-art methods. For baselines from the leader board, team ‘grt123’ and ‘J. de Wit & D. Hammack’ contained contextual information in their input image. Specifically, ‘grt123’ extracted nodule’s and contextual features together by a 2×2 pooling, ‘J. de Wit & D. Hammack’ used multiple tasks framework to jointly learn different attributes and nodule’s

malignancy. Whether using contextual information was not described in the competition reports of team ‘Aidence’, ‘qfpxfd’, and ‘Pieere Fillard’. ‘Aidence’ used a multiple tasks learning framework. ‘qfpxfd’, and ‘Pieere Fillard’ adopted boosting methods to ensemble models trained with different settings. For other methods, MV-KBC [40] did not consider contextual information. They designed a 2D multi-view network to jointly learn the nodule’s texture, internal characteristics, and margin. Ozdemir *et al.* [41] used a 3D probabilistic model, where nodule’s and contextual features were extracted together by a global average pooling. Liao *et al.* [42] was the extended version of team ‘grt123’ with refined optimization strategy.

Numerical results are reported in Tab. I. As we can see, our Context-LGM reaches an AUC of 90.24%, outperforming the state-of-the-art baseline by 3.2%. The distribution of predicted cancer probability is shown by the ROC curve in Fig. 4, it can be further concluded that our method achieves better performance under almost all TP/FP rate settings. These results provide a strong verification of our method’s effectiveness.

Emotion Recognition. For our compared baselines, Efficient-Face [48] and MA-Net [49] only considered facial features. Specifically, EfficientFace learned local and global face features by a local feature extractor and a channel-spatial modulator. MA-Net proposed to learn facial features by a multi-level attention mechanism. Other baselines were methods taking both facial and contextual features into consideration. CAER-Net [43] and Jaiswal *et al.* [44] both proposed to use spatial-wise attention mechanism to capture context. Zeng *et al.* [45]

Method	Publish	Applications	DSB2017(AUC)	CAER-S(Acc)
SPP [6]	ECCV 14	image classification, object detection	88.63 ± 0.27	77.10 ± 0.16
PSP [50]	CVPR 17	scene parsing	88.76 ± 0.04	84.25 ± 0.11
Multi-Crop* [7]	PR 17	image classification	89.02 ± 0.15	83.23 ± 0.41
DeepLab v3+ [8]	ECCV 18	semantic segmentation	88.94 ± 0.13	80.90 ± 0.22
A ² -Net [10]	NeurIPS 18	image/video classification	89.28 ± 0.05	82.89 ± 0.35
Context-Enc [51]	CVPR 18	semantic segmentation, image classification	89.23 ± 0.09	83.84 ± 0.02
Non-Local* [9]	CVPR 18	image/video classification, instance segmentation, pose estimation	89.02 ± 0.24	82.36 ± 0.41
SE-Net* [11]	CVPR 18	image classification	89.28 ± 0.31	83.52 ± 0.16
Stand-Alone* [12]	NeurIPS 19	image classification, object detection	89.40 ± 0.27	83.45 ± 0.93
LR-Net* [13]	ICCV 19	image classification	89.12 ± 0.25	84.46 ± 0.18
Asy Non-Local [52]	ICCV 19	semantic segmentation	89.07 ± 0.32	79.78 ± 0.69
AA-Conv* [14]	ICCV 19	image classification, object detection	89.24 ± 0.32	82.58 ± 0.13
GloRe* [15]	CVPR 19	image classification, semantic segmentation, action recognition	88.83 ± 0.68	<u>84.65</u> ± 0.97
DA-Net [53]	CVPR 19	scene parsing	88.94 ± 0.38	82.30 ± 0.44
LCT* [17]	AAAI 20	image classification, object detection	89.06 ± 0.43	84.34 ± 0.24
CaC-Net [54]	ECCV 20	semantic segmentation	89.37 ± 0.02	77.86 ± 0.49
Att Deeplab v3+ [55]	ECCV 20	lesion segmentation	89.01 ± 0.11	82.23 ± 0.12
ECA-Net* [16]	CVPR 20	image classification, object detection, instance segmentation	<u>89.41</u> ± 0.14	83.99 ± 0.59
CG-Net [56]	TIP 21	semantic segmentation	88.90 ± 0.71	83.16 ± 0.11
RCAM [57]	CVPR 21	glass surface detection	88.66 ± 0.10	77.91 ± 0.54
CGT* [18]	CVPR 21	image classification, object detection	88.70 ± 0.34	83.91 ± 0.58
ours			90.24 ± 0.16	85.30 ± 0.07

TABLE IV

RESULTS OF REPLACING OUR CONTEXTUAL POSTERIOR TRANSFORMER WITH OTHER NON OBJECT-CONTEXT CORRELATION CONTEXT MODELING METHODS WHEN ESTIMATE CONTEXTUAL LATENT z_c . * BEHIND A METHOD’S NAME DENOTES THE METHOD IS ORIGINALLY USED AS A CONTEXT BLOCK INSIDE THE CONVOLUTIONAL BACKBONE. RESULTS ARE REPORTED IN MEAN ± STD.

layers number	DSB2017(AUC)	CAER-S(Acc)
1	89.95 ± 0.42	85.30 ± 0.07
2	90.24 ± 0.16	84.13 ± 0.12
3	89.20* ± 0.04	84.41 ± 0.12

TABLE V

INFLUENCE OF TRANSFORMER LAYERS NUMBER. * DENOTES USING NVIDIA APEX LIBRARY TO CONDUCT FP16/FP32 MIXED PRECISION TRAINING DUE TO GPU MEMORY CONSTRAINTS.

heads number	DSB2017(AUC)	CAER-S(Acc)
1	89.98 ± 0.05	85.08 ± 0.05
2	90.00 ± 0.06	85.30 ± 0.07
4	90.24 ± 0.16	84.97 ± 0.13
8	89.26* ± 0.02	84.92 ± 0.12

TABLE VI

INFLUENCE OF TRANSFORMER HEADS NUMBER. * DENOTES USING NVIDIA APEX LIBRARY TO CONDUCT FP16/FP32 MIXED PRECISION TRAINING DUE TO GPU MEMORY CONSTRAINTS.

designed a graph convolution network to capture semantic relationships among different small contextual regions. SIB-Net [46] constructed a recurrent neural network to propagate the sequential influence in a face-body-scene order. Li *et al.* [47] also explored regions that contribute more to the emotion, without explicitly model of the object-context relation.

Comparison results are shown in Tab. II. As we can see, our method reaches a Top-1 Accuracy of 85.30%/91.36% under different backbone settings, which outperforms state-of-the-art baselines by 4.0%/2.9%, respectively. These results further demonstrate the effectiveness of our methods.

D. Ablative Study

In this section, we conduct ablative experiments to achieve a better understanding of the effect of each component in our Context-LGM. As shown in Tab. III, the improvement compared to the vanilla cross-entropy method mainly comes from the latent generative model (VAE) that explicitly models the object-context correlation, as well as its following contextual posterior Transformer equipped with modified attention function to select contextual factors that are highly correlated with the object. These results indicate the importance of modeling the relation between contextual features and the object.

E. Comparison with Other Methods in Learning z_c

To further validate the superiority of incorporating object-context relation, we compare with other non object-context relation methods by replacing our Transformer with them when inferring z_c . These methods, as categorized based on their applications, include context blocks in neural architectures designs [7], [9], [11]–[17], image classification [6], [7], [10]–[17], detection [57], segmentation [8], [51], [52], [54]–[56], scene parsing [50], [53] and action recognition [15]. Their corresponding context modeling methods contain stacking of different sizes feature maps [6], [7], [50], atrous convolution [8], spatial-wise attention [9], [12]–[14], channel-wise attention [11], [16], [17], [51], spatial-channel wise attention [10], [53], [54], graph based spatial attention [15]. Some of these works combined two of different types context modeling methods, such as [52] combined features pyramid with spatial-wise attention, [55]–[57] combined atrous convolution with

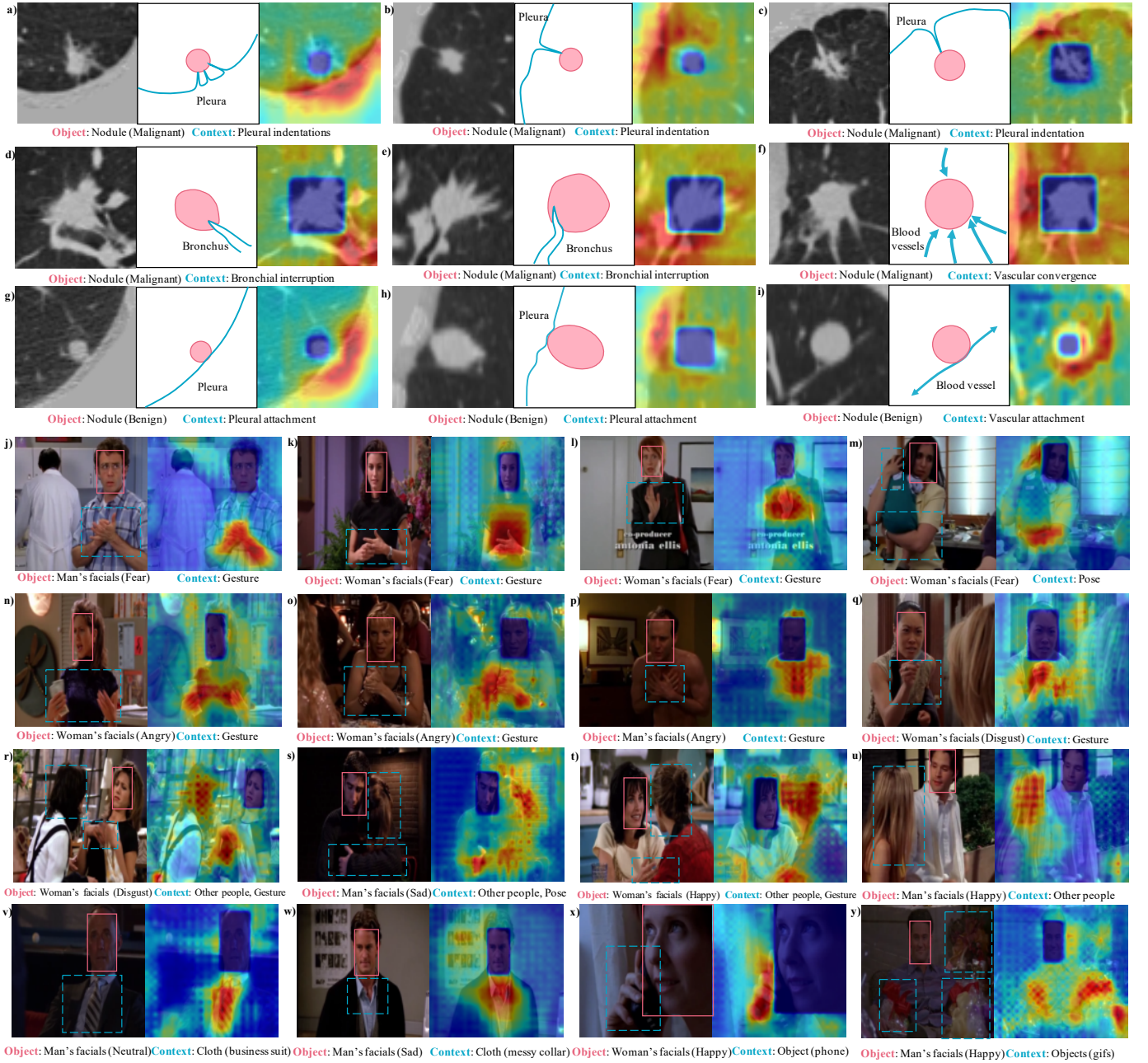


Fig. 5. Visualization of the learned object-context correlation matrices. For each example, the left image shows the input x to our Context-LGM, and the right image shows the computed correlation matrix. Object regions in the correlation matrix are with zero response. This is because we mask them in F_{mask} to avoid interference from object-object correlation.

channel-wise attention. All these methods only exploit object’s label to supervise the learning of contextual feature; *that is*, they overlook the importance of object-context relation.

As observed in Tab. IV, our contextual posterior Transformer outperforms all the other methods by a noticeable margin (0.8%-1.2% in lung cancer prediction and 0.6%-6.0% in emotion recognition). These results show that, due to the diversity of contextual features, the existing methods may fail to capture them comprehensively; **in contrast**, the exploitation of an extra inductive bias, *i.e.* object-context relation, enables our method to capture them well.

F. Hyper-parameters Analysis

In this section, we examine the influence of hyper-parameters on our contextual posterior Transformer.

Layers Number. The results are shown in Tab. V. It can be observed that our Transformer reaches satisfactory results when the layers number is 2 for lung cancer prediction or 1 for emotion recognition. As a matter of fact, since using more layers could significantly increase computation costs, similar layers number setting are also reported in some other visual Transformers, such as [37] use 1 layer, [60], [61] uses 3 layers.

Heads Number. Multi-head mechanism is introduced in Transformer to model various aspects of contextual relation-

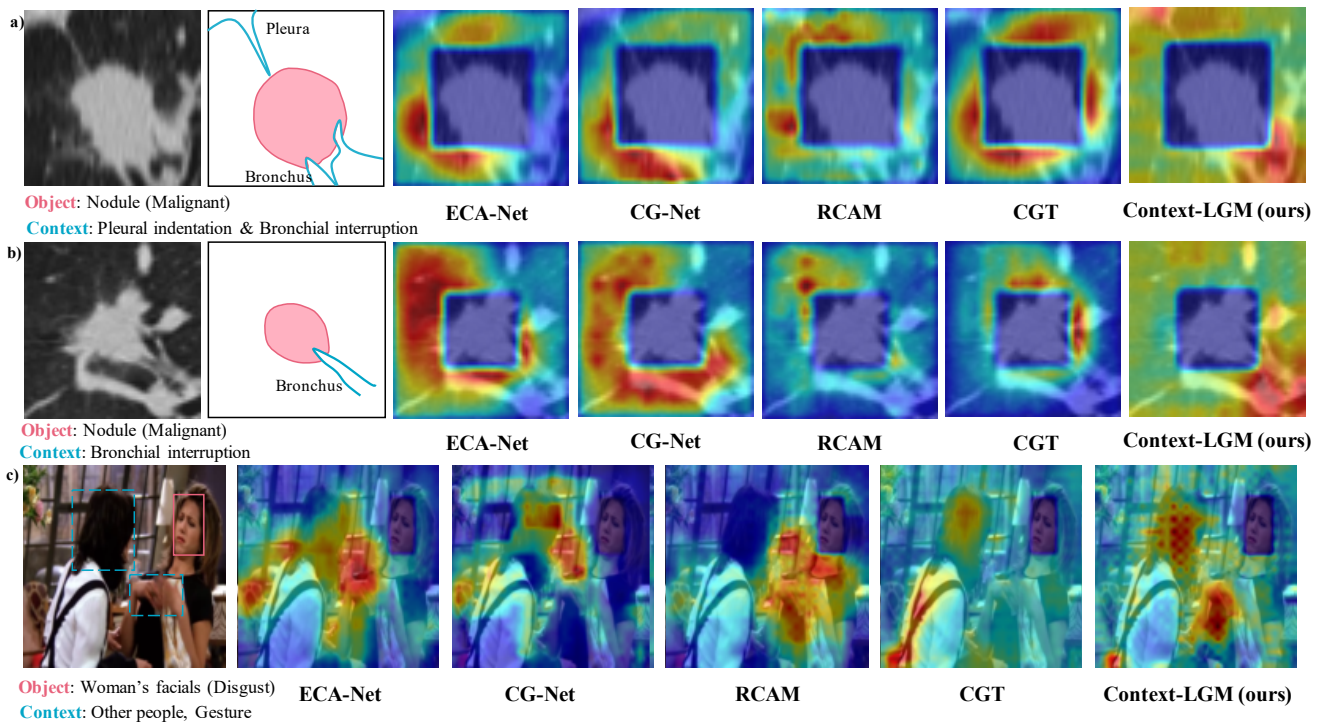


Fig. 6. Visualization of learned context in different methods.

ships. We conduct experiments on different heads number and report the results in Tab. VI. We can see that our model reaches the best performance when $n_h = 4$ for lung cancer prediction and $n_h = 2$ for emotion recognition. This may be because contextual features in lung cancer are more complicated than those in emotion. As an intuitive example, in emotion recognition, there may be at most two types of contextual features (*i.e.* gestures, other people) presenting together. However, in lung cancer, the malignant nodule can cause multiple pleural indentations (Fig. 7-a) or vascular convergence (Fig. 5-f) at the same time.

G. Visualization

In Context-LGM, we use object-context correlation as extra information to locate contextual factors. Such a correlation is parameterized by the cross-attention block in our Transformer. This block computes a correlation matrix between object z_c and surrounding regions in F_{mask} . Regions with high correlation values are contextual factors, while those with low correlation values are backgrounds.

Learned Correlation Matrix. We visualize the correlation metrics in Fig. 5. For each example, the left image is the input x to our Context-LGM, and the right image shows the computed correlation matrix. In the correlation matrix, a large value indicates a high correlation with the object. The object regions are with zero response. This is because we mask them in F_{mask} to avoid interference from object-object correlations.

We can observe that regions with contextual features show high correlation response, and those without context show low response. For example, in lung nodule related context, indentation to bottom right pleura in Fig. 5(a), and indentation

to the left upper pleura in Fig. 5(b,c) are captured by high response correlation. In Fig. 5(d,e), the bronchial interruption context in the nodule's bottom areas is emphasized. In Fig. 5(f), the vascular convergence context is emphasized, too. Also, the pleural and vascular attachment context are well captured by object-context correlation in Fig. 5(g-i). In facial emotion related context, various of human gestures (Fig. 5-j,k,l,n,o,p,q) and posture (Fig. 5-m) are well captured by our object-context correlation. In Fig. 5(r-u), our method learns correlation between the target face and other people. In Fig. 5(v,w), it can be seen that our object-context correlation is also able to capture the clothing context (business suit with serious facials, messy collar with sad facials). Also, context from environmental objects such as phones and gifts are well capture in Fig. 5(x,y).

From these observations, we could conclude that our object-context correlation mainly looks at contextual regions in an object's surroundings, thus well promote the learning of contextual representations.

Comparison with Other Methods. We also compare with context captured by other methods and show the results in Fig. 6. As we can see, only our Context-LGM correctly capture the pleural indentation and bronchial interruption context in Fig. 6(a) and the bronchial interruption context in Fig. 6(b). In Fig. 6(c), only our method comprehensively captures both the gesture and other people context. Such a more accurate and comprehensive capturing of context further verify the effectiveness of using object-context relation, as well as the use of multi-head attention as implementation.

Roles of Different Heads. Each of our cross-attention block composites multiple attention heads ($n_h = 4$ in lung cancer

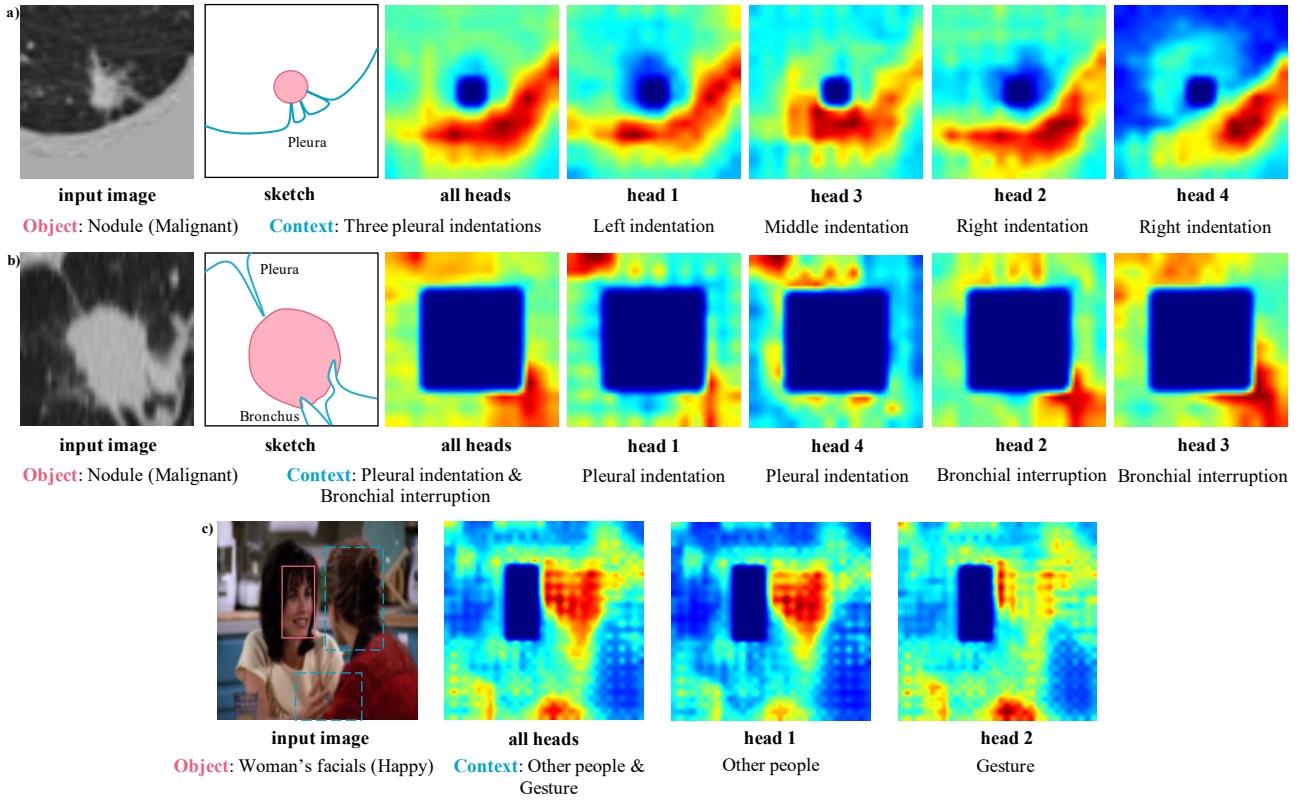


Fig. 7. Comparison of correlation matrices in different attention heads.

prediction and $n_h = 2$ in emotion recognition, specifically). This mechanism could enhance representation powers on different aspects of contextual information. To show the roles of different attention heads and how do they work together, we present visualization examples of correlation metrics in different attention heads in Fig. 7

It can be observed that different heads seem to focus on different regions. For example, nodule in Fig. 7(a) shows three indentations to its bottom right pleura. It seems that head 1 mainly looks at the left indentation, head 3 focuses on the middle indentation, and heads 2, 4 mainly correlate with the right indentation. In Fig. 7(b), the nodule shows both pleural indentation context in the upper left and bronchial interruption context in the right bottom. It seems that heads 1, 4 focus on correlation with the first context regions, and heads 2, 3 focus on correlation with the second context regions. In Fig. 7(c), contextual factors include both the target women's gesture and other people. It seems that head 1 mainly looks at the other people context, and head 2 focuses on the gesture context.

Such an observation indicates complementary cooperation may be learned among different attention heads. This mechanism could be especially beneficial when multiple contextual regions exist.

V. CONCLUSION

In this paper, we propose Context-LGM, a novel latent generative model for context-aware object recognition. We firstly incorporate the object-context relation via their generating processes in the latent generative model. Then, we design a

reformulated VAE framework, within which a carefully modified Transformer is equipped to take the object's information as a reference and infer contextual features. Our method can achieve state-of-the-art results on lung nodule prediction and emotion recognition. Moreover, the learned context features are highly explainable.

We believe that the object-context relation, as widely exists in other vision tasks such as scene understanding, action recognition, and human-computer interaction, can serve a broader family of applications. We leave this exploration in the future work.

APPENDIX A PATHOLOGICAL BACKGROUND

Though context in the natural image is easy to understand, it takes some background knowledge to understand it in the medical image. To give an intuition, we provide radiological examples about the common context in lung cancer prediction.

In Fig. 8, (a-c) show context correlated with malignant nodules, and (d-e) show context correlated with benign nodules.

Specifically, **pleural indentation** [1] in Fig. 8(a) represents pulling the visceral pleura towards the nodule. It suggests a possible pleural invasion by peripheral lung tumor. Invasion and contractile changes of the tumor cause dead space, then the linear strand between tumor and pleural is formed by compensatory expansion of lung tissues to fill the dead space; **vascular convergence** [2] in Fig. 8(b) is described as vessels converging towards a nodule. This is because angiogenesis is essential for tumor growth and metastasis. The vascular endothelial growth

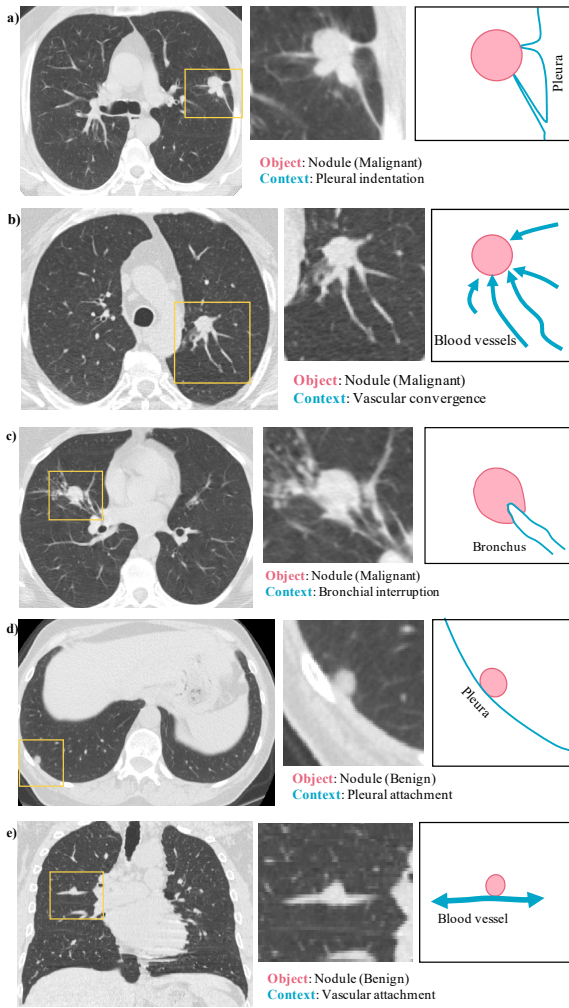


Fig. 8. Radiological examples for context in lung cancer prediction.

factor is then synthesized continuously and excessively in the tumor, promoting the proliferation of vascular endothelial cells during vessel formation; **bronchial interruption** [62] in Fig. 8(c) means the bronchus is obstructed abruptly by the tumor or it penetrates into the tumor with tapered narrowing and interruption. This context is resulted by the growth pattern of malignant nodules, i.e. the hilic growth and the lepidic growth. In hilic growth, the tumor cells proliferate and pile up continuously, forming a solid mass and obstruct adjacent bronchus. In lepidic growth, the tumor cells line the alveolar wall and directly spread from one alveolus to another through the pore of Köhn. Thus the bronchus remains intact and penetrates into the mass. **Pleural attachment** in Fig. 8(d), and **vascular attachment** in Fig. 8(e) respectively represent that the nodule is adjacent to a pleura or blood vessel. Their relation to benignity are mainly confirmed by clinical statistics [63].

ACKNOWLEDGMENT

The work is supported in part by NSFC Grants (No. 61625201), MOST Grants (No. 2018AAA0102004), and the Beijing Municipal Science and Technology Planning Project (No. Z201100005620008).

REFERENCES

- [1] N. Seki, Y. Fujita, R. Shibakuki, T. Seto, K. Uematsu, and K. Eguchi, "Easier understanding of pleural indentation on computed tomography," *Internal Medicine*, vol. 46, no. 24, pp. 2029–2030, 2007. **I, A**
- [2] H. Hu, Q. Wang, H. Tang, L. Xiong, and Q. Lin, "Multi-slice computed tomography characteristics of solitary pulmonary ground-glass nodules: Differences between malignant and benign," *Thoracic Cancer*, vol. 7, no. 1, pp. 80–87, 2016. **I, A**
- [3] J. V. den Stock, R. Righart, and B. de Gelder, "Body expressions influence recognition of emotions in the face and voice," *Emotion*, vol. 7, no. 3, pp. 487–494, 2007. **I**
- [4] M. J. Wieser and T. Brosch, "Faces in context: A review and systematization of contextual influences on affective face processing," *Frontiers in Psychology*, vol. 3, 2012. **I**
- [5] L. F. Barrett and E. A. Kensinger, "Context is routinely encoded during emotion perception," *Psychological Science*, vol. 21, no. 4, pp. 595–599, 2010. **I**
- [6] K. He, X. Zhang, S. Ren, and J. Sun, "Spatial pyramid pooling in deep convolutional networks for visual recognition," in *Computer Vision – ECCV 2014*, 2014, pp. 346–361. **I, II-A, II-A, IV, IV-E, IV-E**
- [7] W. Shen, M. Zhou, F. Yang, D. Yu, D. Dong, C. Yang, Y. Zang, and J. Tian, "Multi-crop convolutional neural networks for lung nodule malignancy suspiciousness classification," *Pattern Recognition*, vol. 61, pp. 663–673, Jan. 2017. **I, II-A, II-A, IV, IV-E, IV-E**
- [8] L.-C. Chen, Y. Zhu, G. Papandreou, F. Schroff, and H. Adam, "Encoder-decoder with atrous separable convolution for semantic image segmentation," in *Computer Vision – ECCV 2018*, 2018, pp. 833–851. **I, II-A, II-A, IV, IV-E, IV-E**
- [9] X. Wang, R. Girshick, A. Gupta, and K. He, "Non-local neural networks," in *2018 IEEE/CVF Conference on Computer Vision and Pattern Recognition*, 2018, pp. 7794–7803. **I, II-A, II-A, II-A, IV, IV-E, IV-E**
- [10] Y. Chen, Y. Kalantidis, J. Li, S. Yan, and J. Feng, "A²-nets: Double attention networks," in *Advances in Neural Information Processing Systems*, vol. 31, 2018. **I, II-A, II-A, II-A, IV, IV-E, IV-E**
- [11] J. Hu, L. Shen, and G. Sun, "Squeeze-and-excitation networks," in *2018 IEEE/CVF Conference on Computer Vision and Pattern Recognition*, 2018, pp. 7132–7141. **I, II-A, II-A, II-A, IV, IV-E, IV-E, IV-E**
- [12] P. Ramachandran, N. Parmar, A. Vaswani, I. Bello, A. Levskaya, and J. Shlens, "Stand-alone self-attention in vision models," in *Advances in Neural Information Processing Systems*, vol. 32, 2019. **I, II-A, II-A, II-A, IV, IV-E, IV-E, IV-E**
- [13] H. Hu, Z. Zhang, Z. Xie, and S. Lin, "Local relation networks for image recognition," in *2019 IEEE/CVF International Conference on Computer Vision (ICCV)*, 2019, pp. 3463–3472. **I, II-A, II-A, II-A, IV, IV-E, IV-E, IV-E**
- [14] I. Bello, B. Zoph, Q. Le, A. Vaswani, and J. Shlens, "Attention augmented convolutional networks," in *2019 IEEE/CVF International Conference on Computer Vision (ICCV)*, 2019, pp. 3285–3294. **I, II-A, II-A, II-A, IV, IV-E, IV-E, IV-E**
- [15] Y. Chen, M. Rohrbach, Z. Yan, Y. Shuicheng, J. Feng, and Y. Kalantidis, "Graph-based global reasoning networks," in *2019 IEEE/CVF Conference on Computer Vision and Pattern Recognition (CVPR)*, 2019, pp. 433–442. **I, II-A, II-A, II-A, IV, IV-E, IV-E, IV-E, IV-E**
- [16] Q. Wang, B. Wu, P. Zhu, P. Li, W. Zuo, and Q. Hu, "Eca-net: Efficient channel attention for deep convolutional neural networks," in *2020 IEEE/CVF Conference on Computer Vision and Pattern Recognition (CVPR)*, 2020, pp. 11 531–11 539. **I, II-A, II-A, II-A, IV, IV-E, IV-E, IV-E**
- [17] D. Ruan, J. Wen, N. Zheng, and M. Zheng, "Linear context transform block," in *Proceedings of the AAAI Conference on Artificial Intelligence*, vol. 34, no. 04, Apr. 2020, pp. 5553–5560. **I, II-A, II-A, II-A, IV, IV-E, IV-E, IV-E**
- [18] D. Ruan, D. Wang, Y. Zheng, N. Zheng, and M. Zheng, "Gaussian context transformer," in *Proceedings of the IEEE/CVF Conference on Computer Vision and Pattern Recognition (CVPR)*, June 2021, pp. 15 129–15 138. **I, II-A, II-A, II-A, IV**
- [19] J. L. Davenport and M. C. Potter, "Scene consistency in object and background perception," *Psychological Science*, vol. 15, no. 8, pp. 559–564, 2004. **I**
- [20] H. K. Meerlen, C. C. van Heijnsbergen, and B. de Gelder, "Rapid perceptual integration of facial expression and emotional body language," *Proc. Natl. Acad. Sci. U. S. A.*, vol. 102, no. 45, pp. 16 518–16 523, Nov 2005. **I**
- [21] A. Vaswani, N. Shazeer, N. Parmar, J. Uszkoreit, L. Jones, A. N. Gomez, L. u. Kaiser, and I. Polosukhin, "Attention is all you need," in *Advances in Neural Information Processing Systems*, vol. 30, 2017. **I, II-C, III-C**

- [22] M. Liu, F. Zhang, X. Sun, Y. Yu, and Y. Wang, "Ca-net: Leveraging contextual features for lung cancer prediction," in *Medical Image Computing and Computer Assisted Intervention – MICCAI 2021*, 2021, pp. 23–32. **I**
- [23] I. Higgins, L. Matthey, A. Pal, C. Burgess, X. Glorot, M. Botvinick, S. Mohamed, and A. Lerchner, "beta-vae: Learning basic visual concepts with a constrained variational framework," 2016. **II-B, II-B**
- [24] T. Q. Chen, X. Li, R. B. Grosse, and D. K. Duvenaud, "Isolating sources of disentanglement in variational autoencoders," in *NeurIPS*, 2018. **II-B, II-B**
- [25] J. Li, B. Wu, X. Sun, and Y. Wang, "Causal hidden markov model for time series disease forecasting," in *Proceedings of the IEEE/CVF Conference on Computer Vision and Pattern Recognition*, 2021, pp. 12 105–12 114. **II-B**
- [26] X. Sun, B. Wu, C. Liu, X. Zheng, W. Chen, T. Qin, and T.-y. Liu, "Latent causal invariant model," *arXiv preprint arXiv:2011.02203*, 2020. **II-B, II-B**
- [27] Z. Ding, Y. Xu, W. Xu, G. Parmar, Y. Yang, M. Welling, and Z. Tu, "Guided variational autoencoder for disentanglement learning," in *Proceedings of the IEEE/CVF Conference on Computer Vision and Pattern Recognition*, 2020, pp. 7920–7929. **II-B**
- [28] S. Mahajan and S. Roth, "Diverse image captioning with context-object split latent spaces," *arXiv preprint arXiv:2011.00966*, 2020. **II-B**
- [29] A. Dosovitskiy, L. Beyer, A. Kolesnikov, D. Weissenborn, X. Zhai, T. Unterthiner, M. Dehghani, M. Minderer, G. Heigold, S. Gelly, J. Uszkoreit, and N. Houlsby, "An image is worth 16x16 words: Transformers for image recognition at scale," in *International Conference on Learning Representations*, 2021. **II-C**
- [30] H. Touvron, M. Cord, M. Douze, F. Massa, A. Sablayrolles, and H. Jegou, "Training data-efficient image transformers amp distillation through attention," in *Proceedings of the 38th International Conference on Machine Learning*, vol. 139, 2021, pp. 10 347–10 357. **II-C**
- [31] L. Ye, M. Rochan, Z. Liu, and Y. Wang, "Cross-modal self-attention network for referring image segmentation," in *2019 IEEE/CVF Conference on Computer Vision and Pattern Recognition (CVPR)*, 2019, pp. 10 494–10 503. **II-C**
- [32] A. Kirillov, K. He, R. Girshick, C. Rother, and P. Dollar, "Panoptic segmentation," in *Proceedings of the IEEE/CVF Conference on Computer Vision and Pattern Recognition (CVPR)*, June 2019. **II-C**
- [33] Y. Wang, Z. Xu, X. Wang, C. Shen, B. Cheng, H. Shen, and H. Xia, "End-to-end video instance segmentation with transformers," in *Proceedings of the IEEE/CVF Conference on Computer Vision and Pattern Recognition (CVPR)*, June 2021, pp. 8741–8750. **II-C**
- [34] N. Carion, F. Massa, G. Synnaeve, N. Usunier, A. Kirillov, and S. Zagoruyko, "End-to-end object detection with transformers," in *Computer Vision – ECCV 2020*, 2020, pp. 213–229. **II-C**
- [35] D. Neimark, O. Bar, M. Zohar, and D. Asselmann, "Video transformer network," *arXiv preprint arXiv:2103.10455*, 2021. **II-C**
- [36] X. Ma, J. Su, C. Wang, H. Ci, and Y. Wang, "Context modeling in 3d human pose estimation: A unified perspective," in *Proceedings of the IEEE/CVF Conference on Computer Vision and Pattern Recognition (CVPR)*, June 2021, pp. 6238–6247. **II-C**
- [37] N. Wang, W. Zhou, J. Wang, and H. Li, "Transformer meets tracker: Exploiting temporal context for robust visual tracking," in *Proceedings of the IEEE/CVF Conference on Computer Vision and Pattern Recognition (CVPR)*, June 2021, pp. 1571–1580. **II-C, III-C, IV-F**
- [38] C. Plizzari, M. Cannici, and M. Matteucci, "Skeleton-based action recognition via spatial and temporal transformer networks," *Computer Vision and Image Understanding*, vol. 208, p. 103219, 2021. **II-C**
- [39] K. H. Greenaway, E. K. Kalokerinos, and L. A. Williams, "Context is everything (in emotion research)," *Social and Personality Psychology Compass*, vol. 12, no. 6, p. e12393, 2018. **III-A**
- [40] Y. Xie, Y. Xia, J. Zhang, Y. Song, D. Feng, M. Fulham, and W. Cai, "Knowledge-based collaborative deep learning for benign-malignant lung nodule classification on chest ct," *IEEE Transactions on Medical Imaging*, vol. 38, no. 4, pp. 991–1004, 2019. **IV, IV-C**
- [41] O. Ozdemir, R. L. Russell, and A. A. Berlin, "A 3d probabilistic deep learning system for detection and diagnosis of lung cancer using low-dose ct scans," *IEEE Transactions on Medical Imaging*, vol. 39, no. 5, pp. 1419–1429, 2020. **IV, IV-C**
- [42] F. Liao, M. Liang, Z. Li, X. Hu, and S. Song, "Evaluate the malignancy of pulmonary nodules using the 3-d deep leaky noisy-or network," *IEEE Transactions on Neural Networks and Learning Systems*, vol. 30, no. 11, pp. 3484–3495, 2019. **IV-B, IV, IV-C**
- [43] J. Lee, S. Kim, S. Kim, J. Park, and K. Sohn, "Context-aware emotion recognition networks," in *2019 IEEE/CVF International Conference on Computer Vision (ICCV)*, 2019, pp. 10 142–10 151. **IV-A, IV-B, IV, IV-C**
- [44] S. Jaiswal, S. Misra, and G. Nandi, "Attention-guided context-aware emotional state recognition," in *2020 IEEE 7th Uttar Pradesh Section International Conference on Electrical, Electronics and Computer Engineering (UPCON)*, 2020, pp. 1–6. **IV-B, IV, IV-C**
- [45] H. Zeng, G. Li, T. Tong, and Q. Gao, "A graph convolutional network for emotion recognition in context," in *2020 Cross Strait Radio Science Wireless Technology Conference (CSRSWTC)*, 2020, pp. 1–3. **IV-B, IV, IV-C**
- [46] X. Li, X. Peng, and C. Ding, "Sequential interactive biased network for context-aware emotion recognition," in *2021 IEEE International Joint Conference on Biometrics (IJCB)*, 2021, pp. 1–6. **IV-B, IV, IV-C**
- [47] W. Li, X. Dong, and Y. Wang, "Human emotion recognition with relational region-level analysis," *IEEE Transactions on Affective Computing*, pp. 1–1, 2021. **IV-B, IV, IV-C**
- [48] Z. Zhao, Q. Liu, and F. Zhou, "Robust lightweight facial expression recognition network with label distribution training," in *Proceedings of the AAAI Conference on Artificial Intelligence*, vol. 35, no. 4, 2021, pp. 3510–3519. **IV-B, IV, II, IV-C**
- [49] Z. Zhao, Q. Liu, and S. Wang, "Learning deep global multi-scale and local attention features for facial expression recognition in the wild," *IEEE Transactions on Image Processing*, vol. 30, pp. 6544–6556, 2021. **IV-B, IV, IV-C**
- [50] H. Zhao, J. Shi, X. Qi, X. Wang, and J. Jia, "Pyramid scene parsing network," in *2017 IEEE Conference on Computer Vision and Pattern Recognition (CVPR)*, 2017, pp. 6230–6239. **IV, IV-E, IV-E**
- [51] H. Zhang, K. Dana, J. Shi, Z. Zhang, X. Wang, A. Tyagi, and A. Agrawal, "Context encoding for semantic segmentation," in *2018 IEEE/CVF Conference on Computer Vision and Pattern Recognition*, 2018, pp. 7151–7160. **IV, IV-E, IV-E**
- [52] Z. Zhu, M. Xu, S. Bai, T. Huang, and X. Bai, "Asymmetric non-local neural networks for semantic segmentation," in *2019 IEEE/CVF International Conference on Computer Vision (ICCV)*, 2019, pp. 593–602. **IV, IV-E, IV-E**
- [53] J. Fu, J. Liu, H. Tian, Y. Li, Y. Bao, Z. Fang, and H. Lu, "Dual attention network for scene segmentation," in *2019 IEEE/CVF Conference on Computer Vision and Pattern Recognition (CVPR)*, 2019, pp. 3141–3149. **IV, IV-E, IV-E**
- [54] J. Liu, J. He, Y. Qiao, J. S. Ren, and H. Li, "Learning to predict context-adaptive convolution for semantic segmentation," in *Computer Vision – ECCV 2020*, 2020, pp. 769–786. **IV, IV-E, IV-E**
- [55] R. Azad, M. Asadi-Aghbolaghi, M. Fathy, and S. Escalera, "Attention deeplabv3+: Multi-level context attention mechanism for skin lesion segmentation," in *Computer Vision – ECCV 2020 Workshops*, 2020, pp. 251–266. **IV, IV-E, IV-E**
- [56] T. Wu, S. Tang, R. Zhang, J. Cao, and Y. Zhang, "Cgnet: A light-weight context guided network for semantic segmentation," *IEEE Transactions on Image Processing*, vol. 30, pp. 1169–1179, 2021. **IV, IV-E, IV-E**
- [57] J. Lin, Z. He, and R. W. Lau, "Rich context aggregation with reflection prior for glass surface detection," in *Proceedings of the IEEE/CVF Conference on Computer Vision and Pattern Recognition (CVPR)*, June 2021, pp. 13 415–13 424. **IV, IV-E, IV-E**
- [58] (2017) Data science bowl 2017. [Online]. Available: <https://www.kaggle.com/c/data-science-bowl-2017> **IV-A**
- [59] G. Huang, Z. Liu, L. van der Maaten, and K. Q. Weinberger, "Densely connected convolutional networks," in *Proceedings of the IEEE Conference on Computer Vision and Pattern Recognition (CVPR)*, July 2017. **IV-B**
- [60] R. Girdhar, J. Carreira, C. Doersch, and A. Zisserman, "Video action transformer network," in *Proceedings of the IEEE/CVF Conference on Computer Vision and Pattern Recognition (CVPR)*, June 2019. **IV-F**
- [61] F. Yang, H. Yang, J. Fu, H. Lu, and B. Guo, "Learning texture transformer network for image super-resolution," in *IEEE/CVF Conference on Computer Vision and Pattern Recognition (CVPR)*, June 2020. **IV-F**
- [62] J. Qiang, K. Zhou, G. Lu, Q. Wang, X. Ye, S. Xu, and L. Tan, "The relationship between solitary pulmonary nodules and bronchi: multi-slice ct–pathological correlation," *Clinical Radiology*, vol. 59, no. 12, pp. 1121 – 1127, 2004. **A**
- [63] D. M. Xu, H. J. van der Zaag-Loonen, M. Oudkerk, Y. Wang, R. Vliegenhart, E. T. Scholten, J. Verschakelen, M. Prokop, H. J. de Koning, and R. J. van Klaveren, "Smooth or attached solid indeterminate nodules detected at baseline ct screening in the nelson study: Cancer risk during 1 year of follow-up," *Radiology*, vol. 250, no. 1, pp. 264–272, 2009. **A**